JACS
JOURNAL OF THE AMERICAN CHEMICAL SOCIETY
Article
Cite This: J. Am. Chem. Soc. 2018, 140, 9466−9477
pubs.acs.org/JACS

Water Dynamics in Polyacrylamide Hydrogels

Chang Yan,[†,‡] Patrick L. Kramer,[†] Rongfeng Yuan, and Michael D. Fayer*

Department of Chemistry, Stanford University, Stanford, California 94305, United States

Supporting Information

ABSTRACT: Polymeric hydrogels have wide applications including electrophoresis, biocompatible materials, water superadsorbents, and contact lenses. The properties of hydrogels involve the poorly characterized molecular dynamics of water and solutes trapped within the three-dimensional cross-linked polymer networks. Here we apply ultrafast two-dimensional infrared (2D IR) vibrational echo and polarization-selective pump−probe (PSPP) spectroscopies to investigate the ultrafast molecular dynamics of water and a small molecular anion solute, selenocyanate ($SeCN^-$), in polyacrylamide hydrogels. For all mass concentrations of polymer studied (5% and above), the hydrogen-bonding network reorganization (spectral diffusion) dynamics and reorientation dynamics reported by both water and $SeCN^-$ solvated by water are significantly slower than in bulk water. As the polymer mass concentration increases, molecular dynamics in the hydrogels slow further. The magnitudes of the slowing, measured with both water and $SeCN^-$, are similar. However, the entire hydrogen-bonding network of water molecules appears to slow down as a single ensemble, without a difference between the core water population and the interface water population at the polymer−water surface. In contrast, the dissolved $SeCN^-$ do exhibit two-component dynamics, where the major component is assigned to the anions fully solvated in the confined water nanopools. The slower component has a small amplitude which is correlated with the polymer mass concentration and is assigned to adsorbed anions strongly interacting with the polymer fiber networks.

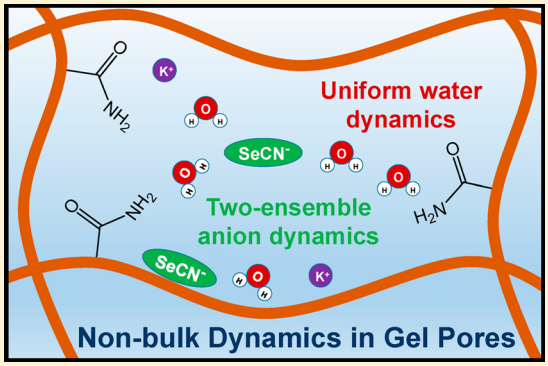

1. INTRODUCTION

In hydrogels, the water mass fraction can approach unity while maintaining a semirigid framework. Microstructures of polymeric hydrogels feature porous networks formed by cross-linked polymer fibers that allow water and dissolved solutes to pass through.[1,2] These properties render polymeric hydrogels useful in a variety of biomedical applications such as tissue engineering,[3,4] wound dressings,[5] and contact lenses.[6] Polymeric hydrogels have also been widely applied for electrophoresis,[7] gel permeation chromatography,[8,9] stimuli-responsive smart materials,[10,11] and self-healing materials.[12,13] Recently, intracellular hydrogel production has been demonstrated.[14]

The molecular dynamics of water and solutes trapped by the gel framework have large impacts on the properties of hydrogel materials. In bulk water, the rearrangements of the hydrogen-bond (H-bond) network show a fast component of ∼400 fs due to local H-bond length fluctuations of intact hydrogen bonds and another slower component of 1.7 ps assigned to the full randomization of the network including H-bond breaking and reformation.[15−20] For water in nonbulk environments, such as the air/water interface,[21,22] water on the surface of biological macromolecules,[23−25] and water confined in reverse micelles,[26−30] the ultrafast dynamics of water molecules are altered as a result of interrupting water's three-dimensional tetrahedral hydrogen-bonding network. In polymeric hydrogels, water molecules are confined by the polymer fibers and will interact with them. Depending on the pore size distribution and the chemical nature of the fibers, dynamics of water molecules and solutes dissolved in the water-filled hydrogel regions can be significantly different from their respective bulk dynamics.

Dielectric relaxation,[31] nuclear magnetic resonance (NMR),[32] neutron scattering methods,[33] and molecular dynamics simulations[34−36] have shown that water confined in the hydrogel framework remains highly mobile, while the dynamics are slowed compared with that of bulk water. Though the previous experiments provide important insights, these methods operate by extracting dynamical data from frequency-domain measurements and thus do not directly measure ultrafast water molecular dynamics. Rather, a model is required to relate the frequency-domain observables to water motion time scales. Ultrafast time-resolved fluorescence experiments probing the solvation dynamics around large aromatic fluorescent molecules in hydrogels have also been reported,[37,38] though these are limited to slower dynamics.

Ultrafast infrared (IR) spectroscopies directly measure water's molecular dynamics with subpicosecond resolution using either water molecules themselves[18,20,39,40] or solutes such as small-size molecular anions[41−43] as vibrational probes. The water and solute dynamics in a variety of nonbulk systems including reverse micelles,[28,44] lipid bilayers,[45,46] concentrated salt solutions,[18,47,48] ionic liquids,[49] and polymer aqueous

Received: April 1, 2018
Published: July 9, 2018

DOI: 10.1021/jacs.8b03547
J. Am. Chem. Soc. 2018, 140, 9466−9477

solutions[43,50] have been investigated with ultrafast IR spectroscopies. Here we apply two-dimensional infrared (2D IR) vibrational echo spectroscopy and IR polarization-selective pump−probe (PSPP) spectroscopy to measure the dynamics of water and a small anion solute, selenocyanate ($SeCN^-$), in a series of polyacrylamide (PAAm) hydrogels. PAAm forms an important class of polymeric hydrogels that have extensive applications in biological electrophoresis.[7] Biopolymers, such as proteins and DNA, have average and fluctuating structures that depend on water's H-bond network and dynamical fluctuations.[51] Understanding the local chemical environments with ultrafast time resolution and with nonperturbative probes in this hydrogel system can thus directly translate into better models for dynamics and conformations when molecules interact with a hydrogel.

The PSPP measurements characterize the molecular dynamics by tracking the orientational dynamics of the hydroxyl[49,52] and nitrile[29] bond axes. The vibrational frequencies of the water hydroxyl stretch and $SeCN^-$ nitrile stretch modes are highly sensitive to hydrogen-bonding configurations. 2D IR experiments measure the structural fluctuations in the hydrogen-bonding network by monitoring spectral diffusion dynamics. Structural changes cause the IR transition frequencies to fluctuate on time scales spanning less than hundreds of femtoseconds to many tens of picoseconds.[53,54]

As depicted in Scheme 1, our measurements reveal that the entire hydrogen-bonding network of water molecules confined in PAAm hydrogels is slowed down as a single component without distinguishing the "core" water, those molecules fully solvated by other waters, from the interfacial water, which directly interacts with polymer fibers. No water with exactly the bulk dynamics remains in the gelled matrix, regardless of PAAm concentration. The water dynamics begin to slow down compared with bulk water when the PAAm mass concentration is at 5% and become significantly slower when the PAAm concentration surpasses 10%. The uniform dynamics are attributed to the unique properties of water that result in jump reorientation rather than small step angular diffusion.[19,55] In jump reorientation many water molecules undergo concerted simultaneous hydrogen-bond rearrangement. In addition, the nonionic amide headgroup has both H-bond donor and acceptor sites that form H bonds with water without disrupting water's three-dimensional H-bond network. The dynamics are compared with previous results obtained from water confined in reverse micelles, which do have a clear separation between bulk-like water and much slower interfacial water.[26−30]

The dynamics of the dispersed small molecular anion solute, $SeCN^-$, slow down as well but exhibit two-component features in the time-resolved measurements. The major component on the time scale of a few picoseconds keeps track of the slow nonbulk water molecules solvating the anion. In addition to this major dynamical component, a much slower component with structural rearrangements taking several tens of picoseconds is attributed to $SeCN^-$ interacting with polymer fibers and thus not being solvated by a three-dimensional water H-bond network.

Scheme 1. Illustration of a Hydrogel Water Nanopool[a]

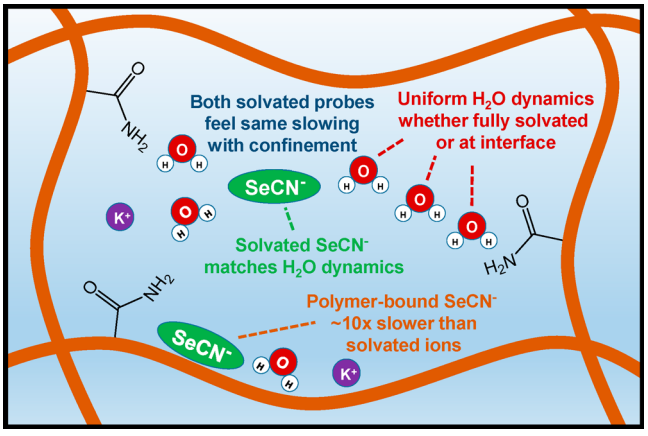

[a]Water molecules are found to slow down as a single dynamical ensemble with increasing confinement. Higher polymer concentrations cause slower water dynamics. Solvated $SeCN^-$ ions slow similarly to the surrounding water, while a second population of polymer-bound ions exhibits much slower dynamics that are independent of PAAm concentration.

2. EXPERIMENTAL METHODS

2.1. Sample Preparation. All chemicals were purchased from Sigma-Aldrich with at least 99% purity and used as received. The PAAm hydrogels were polymerized from an aqueous solution containing acrylamide monomer and *N,N′*-methylenebis(acrylamide) (Bis) cross-linker using ammonium persulfate (APS) as the initiator and *N,N,N′,N′*-tetramethylethylenediamine (TEMED) as the catalyst. The total polymer mass concentration in weight over volume (w/v) in the hydrogels is denoted as *T* (including both acrylamide and Bis), and the weight percentage of the Bis cross-linker in the total polymer mass (w/w) is *C*. In the present study, *C* was maintained as 3.3% and *T* was varied from 5% to 60%.

For the infrared experiments on water, the O−D stretch of 5% HOD solution (singly deuterated water) was used as the probe. The O−D stretch is a local mode that is well separated in frequency from the O−H stretch of HOD and the H_2O solvent. HOD has been shown to report the structural dynamics of the H_2O (or D_2O) H-bond network without the complications of overlapping symmetric and asymmetric stretch vibrations or resonant energy transfer between water molecules in close proximity that exist when studying pure H_2O or D_2O.[15,16,56] For hydrogels containing 5% HOD in H_2O as the water component, we mixed D_2O and H_2O with a volume ratio of 2.5:97.5 and dissolved solid acrylamide and Bis cross-linker in the deuterated water to form the precursor solution with the desired values of *C* and *T*. To 1 mL of the precursor solution, 10 μL of 10% w/v APS solution (in H_2O) and 1 μL of TEMED were added sequentially. Upon the addition of TEMED, a small portion of the solution was transferred onto a 3 mm thick calcium fluoride (CaF_2) window. Then the window with liquid on it was assembled into an IR sample cell before the solution solidified. The cell consists of a 12 μm Teflon spacer separating two identical CaF_2 windows, with the sample sealed inside. Between 5 and 10 min after the addition of TEMED, the solution solidified into a 12 μm gel slab sandwiched between the two CaF_2 windows of the cell. Then the sample cell was dissembled. The gel slab along with the two windows was first placed under a 100% relative humidity environment at 25 °C with vapor from a 5% HOD water source for 1 h. This allowed further polymerization while preventing the gel from drying. Then the gel with windows was immersed under 5% HOD water for 18 h as an incubation step. The spacer between the windows contained holes to allow removable species such as initiator and catalyst to diffuse out from the gel. The gels with windows were taken out of the water, and the outer rims of the windows were sealed with wax so that water could not escape from the gel. With this method, the deuterated hydroxyl IR spectra of the PAAm hydrogel samples remained unchanged for at least 3 weeks of measurement or storage.

DOI: 10.1021/jacs.8b03547
J. Am. Chem. Soc. 2018, 140, 9466−9477

For hydrogels containing potassium selenocyanate (KSeCN) solutes, the water component was pure D_2O, with 99.9% atom % D. The protocol is almost the same as that described above for hydrogels with 5% HOD. During the 18 h incubation step, 0.4 M KSeCN solution in D_2O was used to introduce the selenocyanate probe into the gel. KSeCN cannot be added before polymerization because it reacts with the initiator. The IR spectrum (C−N stretch and water background) of the gel sample remained the same for at least 3 weeks. A completely dried gel sample was produced by placing an initially T = 60% gel slab under a constantly pumped vacuum line for 1 week until no hydroxyl absorption was detectable by Fourier-transform IR (FTIR) measurement.

2.2. PSPP and 2D IR Measurements. In the following we briefly describe the PSPP and 2D IR measurements. Full details on the steady-state and ultrafast IR methodology are provided in the Supporting Information.

In mid-IR PSPP measurements, the transmission of a weaker probe pulse is modulated by prior excitation of an ensemble of vibrational absorbers with a stronger pump pulse.[54,57] The components of the PSPP signal are recorded at varying pump−probe delay times t with the pump polarization set alternately parallel, $S_{\parallel}(t)$, and perpendicular, $S_{\perp}(t)$, to that of the probe.[58] The parallel and perpendicular PSPP signals are affected by isotropic population dynamics and rotational motions of the absorbers. The two polarization measurements can be combined to give the isotropic population relaxation (vibrational lifetime decay),

$$P(t) = S_{\parallel}(t) + 2S_{\perp}(t) \tag{1}$$

and the anisotropy,

$$r(t) = \frac{S_{\parallel}(t) - S_{\perp}(t)}{S_{\parallel}(t) + 2S_{\perp}(t)} = 0.4C_2(t) \tag{2}$$

The anisotropy provides a measurement of $C_2(t)$, the second Legendre polynomial orientational correlation function.[27,28,59]

Orientational correlation decays that are not simply diffusive (single exponential) can appear as biexponentials due to restricted motions.[60−63] The wobbling-in-a-cone model, with a cone of half angle θ_c,[61−63] has been very successful in describing the hindered rotational dynamics of water in confined environments such as biomolecule surfaces,[64] phospholipid bilayers,[46,65] reverse micelles,[26−28,66,67] fuel cell membranes,[66,68] ionic liquids,[49,69] and concentrated salt solutions.[47,70]

The first exponential term is the result of restricted orientational diffusion within the limited range of angles, the cone, with time constant τ_c to an offset S_2^2, the square of a generalized order parameter, determined by the cone angular width. On a longer time scale, unrestricted orientational relaxation (small angle diffusion or jump diffusion) with time constant τ_m randomizes orientations and brings the correlation function to zero:

$$C_2(t) = (S_2^2 + (1 - S_2^2)\exp(-t/\tau_c))\exp(-t/\tau_m) \tag{3}$$

The order parameter gives the cone half angle through

$$S_2 = \frac{1}{2}\cos(\theta_c)(1 + \cos(\theta_c)) \tag{4}$$

while eq 3 allows us to separate the time constants t_1 and t_2 obtained in a biexponential fit into the wobbling correlation time τ_c and the final complete orientational relaxation time τ_m.

In 2D IR spectroscopy, the time dependence of the structure of a system (structural fluctuations) is measured by observing the time dependence of the vibrational frequencies of the vibration under observation. The vibrational frequencies are spread across the inhomogeneously broadened absorption spectrum. Pulses 1 and 2 of the pulse sequence label the initial frequencies of the vibrations (ω_1, the horizontal axis of the 2D spectrum). During T_w, the waiting time between pulses 2 and 3 of the pulse sequence, the structure of the system changes, which causes the initially labeled frequencies to change. Pulse 3 initiates a read out and the echo pulse reports on the final frequencies (ω_3, the vertical axis of the 2D spectrum).[53,54] Spectral diffusion (the frequency evolution), driven by structural fluctuations affecting the frequencies within the inhomogeneous absorption, causes the 2D line shape to evolve from well correlated (elongated) along the diagonal at short waiting times to uncorrelated (round) at long waiting times.

The change in the 2D IR band shape with T_w is quantitatively evaluated using the center line slope (CLS) method.[71−73] The CLS has been shown to be equal to the T_w-dependent part of the normalized frequency−frequency correlation function (FFCF)[72] and in conjunction with the linear absorption spectrum allows determination of the complete FFCF,

$$C(t) = \langle \delta\omega(0)\delta\omega(t)\rangle = \frac{\delta(t)}{T_2} + \sum_k \Delta_k^2 \exp(-t/\tau_k) \tag{5}$$

Here $\delta\omega(t)$ is the instantaneous frequency fluctuation at time t, Δ_k is the contribution of component k to the inhomogeneous broadening, and τ_k is the correlation time for structural evolution of the kth component. The homogeneous line width, $\Gamma = 1/(\pi T_2)$, includes effects of motionally narrowed contributions, vibrational lifetime decay, and molecular reorientation. Additional details on the contributions to the FFCF, CLS method, and determination of the complete FFCF are given in the Supporting Information.

3. RESULTS AND DISCUSSION

3.1. Linear Absorption Spectra of HOD and $SeCN^-$ in Hydrogels. Linear absorption (FTIR) spectra were obtained for the O−D stretching mode of HOD in bulk water and PAAm hydrogels, with total polymer concentration T ranging from 5% to 40% (w/v). Data collection and background-subtraction details for FTIR studies are given in the Supporting Information. The background-subtracted and normalized absorption spectra are displayed in Figure 1A. The linear absorption of 5% HOD in H_2O (black line) has been analyzed in great detail previously, through both experiments and simulations.[15,16,74] It has a center at 2509 cm^{-1} with a 160 cm^{-1} fwhm. At low concentrations of PAAm, 5% and 10% (red and blue lines, respectively), the absorption spectra are basically identical to bulk water (black). At higher concentrations, 25% and 40% (cyan and purple lines, respectively), the peak broadens toward the red side while changing very little from the peak center to the blue side. The finely spaced bumps centered at 2350 cm^{-1} were due to CO_2 absorption in the air.

The hydroxyl stretch frequency is determined by the hydrogen-bond configuration of the water molecule.[16,56,74,75] More or stronger H bonds donated or accepted by a hydroxyl lead to lower frequency. Conversely, fewer or weaker H bonds yield a higher frequency. The distribution of O−D frequencies is directly determined by the distribution of hydrogen-bond configurations.[74] Focusing only on the peak to blue edge of the band, Figure 1A shows that the distribution of O−D stretch absorption frequencies is nearly identical between bulk water and the hydrogels of various polymer concentrations.

Aside from O−D stretch modes, some $-NH_2$ groups from amides on the polymer backbone will exchange protons with the HOD water to form a population of N−D absorbers. The N−D stretch appears red of the O−D band at ~2485 cm^{-1},[76] and its presence could cause the red side asymmetric broadening at higher PAAm concentrations. While the N−D stretch contributes to the red side of the O−D bands in Figure 1A, its presence did not have any impact on the time-resolved IR studies discussed in the following sections. The vibrational lifetime and anisotropy are evaluated from around the peak through the blue side, where the N−D absorption is negligible

DOI: 10.1021/jacs.8b03547
J. Am. Chem. Soc. 2018, 140, 9466−9477

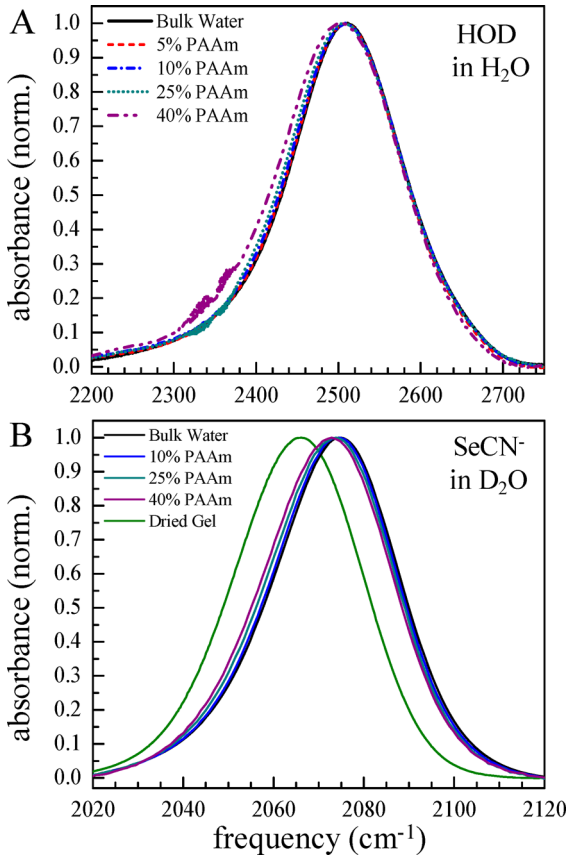

Figure 1. Background-subtracted, normalized absorbance for (A) the O−D stretch of HOD in H_2O for bulk water and hydrogels with PAAm concentrations between 5% and 40% and (B) the nitrile stretch of KSeCN in D_2O for bulk water, hydrogels with PAAm concentrations from 10% to 40%, and the dried gel.

(section 3.2). The 2D IR data are analyzed around the center of the OD stretch spectrum. Thus, the O−D stretch dynamics reported in these experiments are not contaminated by small N−D absorption visible in the linear spectrum.

The FT-IR spectra of $SeCN^-$ dissolved in pure water and hydrogels with various *T* percentages are displayed in Figure 1B. The anion dissolved in bulk D_2O has a spectrum centered at 2075 cm^{-1}. As the total polymer mass concentration is increased, the peak center shifts toward the red side. At *T* = 40%, the peak center is at 2073 cm^{-1}. The peak center of $SeCN^-$ contained in reverse micelles with very low water content shifts to 2065 cm^{-1} due to the lack of anion−water hydrogen bonds.[41] Here, the peak center also shifted to 2066 cm^{-1} for $SeCN^-$ in gels fully dried under vacuum. The small but steady peak shift going from bulk to *T* = 40% indicates that there is a minor, but increasing, population of $SeCN^-$ interacting with a different environment than the H-bonded water network. These anions are likely in close contact with the PAAm polymer fibers. The majority of the anions in the hydrogel are still fully solvated by water as is the case in bulk aqueous solutions. The nitrile stretch of the $SeCN^-$ in bulk water and hydrogels has similar fwhm's in the range of 32.2−33.2 cm^{-1}. The $SeCN^-$ spectra in aqueous environments are asymmetric, with a red wing due to the non-Condon effect: a variation in transition dipole moment with vibrational frequency.[41,77] This further complicates spectral decomposition. The pump−probe measurements (section 3.3) show that the $SeCN^-$ on the polymer fiber "wall" is dynamically different but spectrally very similar to the $SeCN^-$ fully solvated by water.

3.2. Polarization-Selective Pump−Probe Measurements of HOD in H_2O. Population decays for HOD in the various hydrogels were recorded at frequencies spanning from 2490 cm^{-1} (slightly red of the peak at 2509 cm^{-1}) through the entire blue side to 2660 cm^{-1}. The frequency-dependent population decay of the OD stretch of 5% HOD in H_2O (bulk water) was recorded as well. At all detection frequencies and hydrogel concentrations the population decays were fit extremely well by single exponentials. Figure 2A shows the vibrational lifetimes resulting from these fits as a function of detection frequency for the O−D stretch in bulk water and the hydrogels from 5% to 40% PAAm *T* concentration.

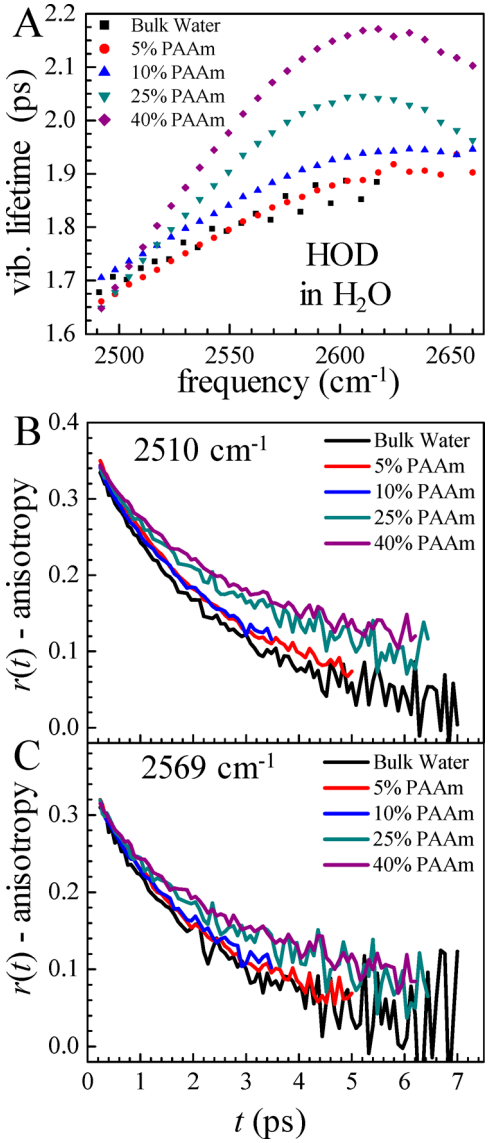

Figure 2. (A) Vibrational lifetime of the O−D stretch of HOD as a function of frequency determined by single-exponential fits to the isotropic pump−probe decays (not shown) for bulk water and hydrogels. (B and C) O−D stretch anisotropy decays for bulk water and hydrogels at (B) the band center (2510 cm^{-1}) and (C) the blue side of the band (2569 cm^{-1}).

DOI: 10.1021/jacs.8b03547
J. Am. Chem. Soc. 2018, 140, 9466−9477

Table 1. Time Constants from Multiexponential Fits to the Anisotropy Decay of the O−D Stretch of HOD and the C−N Stretch of $SeCN^-$ in Bulk Water and Hydrogels with Wobbling-in-a-Cone Analysis of Restricted Orientational Diffusion

sample	t_1 (ps)	τ_c (ps)[a]	θ_c (deg)[b]	$t_2 = \tau_m$ (ps)	$t_3 = \tau_m^{fiber}$ (ps)
HOD in H_2O, global fit across frequencies					
0% PAAm (bulk water)				2.61 ± 0.03	
5% PAAm				2.87 ± 0.04[c]	
10% PAAm	0.8 ± 0.1	1.0 ± 0.2	21 ± 1	3.5 ± 0.1	
25% PAAm	1.1 ± 0.1	1.4 ± 0.2	28 ± 1	6.0 ± 0.3	
40% PAAm	1.5 ± 0.1	1.8 ± 0.2	33 ± 1	8.8 ± 0.7	
$SeCN^-$ in D_2O, fit at peak frequency					
0% PAAm (bulk water)	1.4 ± 0.1	2.0 ± 0.1	21.5 ± 0.4	4.5 ± 0.1	
5% PAAm	1.8 ± 0.1	2.7 ± 0.2	29 ± 1	5.3 ± 0.2	62 ± 3
10% PAAm	1.9 ± 0.1	2.8 ± 0.2	31 ± 1	5.8 ± 0.2	62 ± 3
25% PAAm	1.9 ± 0.1	2.6 ± 0.2	30 ± 1	7.0 ± 0.2	62 ± 3
40% PAAm	2.2 ± 0.1	3.0 ± 0.2	29 ± 1	8.6 ± 0.4	62 ± 3

[a]Wobbling-in-a-cone correlation time given by $\tau_c = (t_1^{-1} - \tau_m^{-1})^{-1}$. [b]Average wobbling cone half angle across detection frequencies for HOD (see Figure S4). Determined at peak center for $SeCN^-$. [c]Average single-exponential time constant across detection frequency range for fit (see Figure S2). Values varied from 2.78 to 2.98 ps.

The vibrational lifetime of the O−D stretch in bulk water is ∼1.8 ps (spanning from 1.7 to 1.9 ps) with a monotonic increase from low frequencies to high frequencies (Figure 2A, black). The vibrational lifetime is very sensitive to the local environment (H-bond interactions), which also determines the vibrational frequency within the inhomogeneously broadened absorption line (Figure 1A). The O−D lifetime is determined by the coupling strength of the hydroxyl stretch to inter- and intramolecular accepting modes and the density of accepting modes in the surroundings.[78] More weakly H-bonded populations (shifted blue from center) tend to have longer vibrational lifetimes, as shown both in Figure 2A and in previous measurements on water in nonbulk environments such as small AOT reverse micelles[27,28] and room-temperature ionic liquids (RTILs).[49,79]

The variation in the lifetimes in all gels and bulk water is relatively small, ranging from just less than 1.7 ps to slightly less than 2.2 ps. As the polymer concentration increases, the variation with wavelength increases. Water molecules will H bond to other water molecules as well as to the polymer. The almost negligible change in the absorption spectra with polymer concentration indicates the range of H-bond strengths for water making one of its four H bonds to the polymer fall within the range of water−water H-bond strengths. However, the vibrational lifetime can be exceedingly sensitive to the nature of intermolecular accepting modes.[78] The increase in the lifetime with polymer concentration indicates that an H bond to the polymer is somewhat less effective at accepting vibrational energy from an OD stretch than are water−water H bonds, though the H bonds to the polymer fall within the range of strengths of water−water H bonds.

In the Supporting Information, parameters of PAAm fibers are used for model calculations of fiber organization in the hydrogels (Table S2). Even at 40% PAAm, only 22% of the water volume is adjacent to polymer fiber, leaving the majority engaged in only water−water H bonds. There is little interfacial water, and it all experiences H bonds to non-interfacial water. Thus, the dynamics of the minor water population interacting with polymer are unlikely to differ from majority population. With these observations as well as the linear absorption spectra (section 3.1), the anisotropy discussed below, and 2D IR observables (section 3.4), we conclude that all of the water molecules contributing to the O−D absorption band act as a single dynamical ensemble with only slight variations in dynamics across detection frequencies caused by the varying H-bond strength within the ensemble.

Anisotropy decays were obtained for bulk water and the hydrogels of varying PAAm concentration over a range of frequencies: from 2490 to 2590 cm^{-1}. The anisotropy, $r(t)$, is proportional to the water orientational correlation function, decaying from a value of 0.4 for complete orientational correlation with the initial excitation to zero for completely randomized orientations. The O−D stretch is a local mode with a transition dipole vector that is almost exactly along the O−D bond direction, so the anisotropy decay directly tracks the rotational motion of the O−D bond vector.[56]

Representative decays are shown in Figure 2B and 2C for O−D stretch frequencies near the peak, 2510 cm^{-1}, and on the blue edge, 2569 cm^{-1}, respectively. The drop from a theoretical maximum value of 0.4 at time zero, which is largest on the blue edge (Figure 2C) and smaller moving red (Figure 2B), is characteristic of hydrogen-bonded oscillators like HOD in bulk water and is similar in the hydrogels. This results from an ultrafast inertial rotational motion that occurs within ∼100 fs, which cannot be measured during the overlap of the pump and probe pulse due to a strong nonresonant signal that tracks the pulse duration.[80] At both frequencies displayed the lower concentration gels (5% and 10%) are seen to exhibit a mild slowing of orientational relaxation compared to the bulk. There is a much more significant slowing on increasing the PAAm concentration to 25% and further to 40%.

While the ultrafast inertial motion time constant cannot be measured, the associated inertial cone angle can be determined from the difference between the maximum possible value of 0.4 and the data at $t = 0$ using eq 4.[49,80,81] Results are plotted for the bulk and all hydrogels in the Supporting Information, Figure S3. The inertial cone half angle has an average of θ_i = 16° for all samples, with a strong dependence on frequency. These cone angles are basically the same within error from bulk water through 40% PAAm, which indicates that the hydrogen-bond strengths are similarly correlated with frequency in the hydrogels as for HOD in pure water. The inertial cone angles and the spectra in Figure 1A show that the range of H-bond strengths in the hydrogels are very similar to those in bulk water.

DOI: 10.1021/jacs.8b03547
J. Am. Chem. Soc. 2018, 140, 9466−9477

HOD in the bulk has a well-known single-exponential anisotropy decay with a 2.6 ps time constant that is independent of detection frequency across the O−D stretch band.[39,40] This time constant is characteristic of water's orientational jump diffusion process, which involves the concerted breaking and reformation of H bonds.[55,82] The hydroxyl undergoes a large angular jump through a bifurcated H-bond transition state to its new configuration.[55,82]

For the bulk water anisotropy, a single-exponential decay was fit globally with one shared time constant across detection frequencies (2492−2590 cm^{-1}), yielding a 2.6 ps reorientation time. All of the hydrogel concentrations have anisotropy decays with some frequency dependence to the dynamics. At 5% PAAm, a single-exponential decay with freely varied time constants across frequencies described the data better than biexponential decays. For 10%, 25%, and 40% hydrogels, however, the data are clearly biexponential and were globally fit sharing the two time constants but varying the amplitudes across the band. The fit results are collected in Table 1. The anisotropy decays in Figure 2B and 2C approach zero by the end of the observable waiting time range and have considerable slope, making the presence of an additional decay with a much slower time constant unlikely. The global fits give excellent agreement with the data at all frequencies. Representative fits for the 40% hydrogel at multiple frequencies are shown in the Supporting Information, Figure S1. Integrated correlation times associated with the fits are shown in Figure S2.

Attempting to fit the anisotropy decays in the hydrogels with a component fixed at the bulk water reorientation rate, with additional exponentials to describe the slower decays, resulted in very poor descriptions of the data. Water with bulk dynamics is not detectable in hydrogels of any PAAm concentration. It is also highly unlikely that the fast component in the anisotropy originates from a distinct population of water molecules interacting directly with the polymer, which should have slower dynamics as seen for $SeCN^-$ anions at the interface (section 3.3). Thus, water was found to change in rotational dynamics as a single dynamical ensemble. The major component which brings the anisotropy to zero slows greatly with increasing PAAm concentration, while a faster motion appears at shorter waiting times.

The biexponential anisotropy for the hydrogels at 10% and above PAAm concentration can be explained as restricted orientational diffusion within a limited cone of angles on shorter time scales, followed by free (jump) diffusion sampling all orientations on a longer time scale.[60−63] Wobbling-in-a-cone half angles for PAAm concentrations of 10%, 25%, and 40% are given in Table 1 as average cone angles over the spectral range for anisotropy measurements. The half angles are plotted as a function of frequency in the Supporting Information, Figure S4. The cone angles show a slight frequency dependence: larger cones at higher frequencies, indicating that weaker H-bonded HOD probes have more freedom to wobble.[49,80] This is the source of the frequency-dependent anisotropy correlation times. The wobbling cone angle, first clearly visible in the 10% hydrogel, becomes larger as the PAAm concentration increases from 25% and 40% (Table 1).

The full orientational randomization time slows dramatically between 2.6 ps in bulk water and 8.8 ps at 40% PAAm (Table 1). For the highest levels of confinement (40% PAAm), the orientational time τ_m is slowed by a factor of 3.4 as compared to bulk water. The hydrogen-bond network becomes much more rigid at medium and high polymer concentrations, slowing down the H-bond exchange which is responsible for complete orientational randomization. Faster motions are still possible without breaking H bonds, however, and the angular cones sampled before the final reorientation period become larger. The time constants for wobbling, τ_c, become larger as the PAAm concentration increases (Table 1). However, the wobbling correlation time is a combination of both the diffusion rate within the cone and the cone angle.[62] The wobbling diffusion constants are the same within error (Table S1). Similar motions in an intact H-bond configuration are sampling a greater range of angles before concerted H-bond rearrangement can occur on the longer time scale for complete orientational randomization, τ_m.

Even at the lowest hydrogel concentration considered, 5% PAAm, the anisotropy decay is slowed measurably from bulk water. It is worthwhile to evaluate this uniform slowdown in terms of the typical size of water pools that exist in the PAAm hydrogels. In the Supporting Information we estimate the water pool size (diameter or spacing between nearest polymer fibers) using two different models: an Ogston model assuming randomly distributed polymer fibers[9,83] and a cubic lattice model with a highly organized fiber arrangement. The lattice model is intended to provide an estimation of the average size rather than literally taking the structure to be a true single-size lattice. Both predict the well-known $T^{-1/2}$ dependence of pore diameter on polymer concentration.[7,9] The results are given as a function of PAAm concentration in Table S2.

While a range of pore or channel sizes must exist in the hydrogels, the mean diameters as calculated here are helpful for understanding the majority (number or volume) of confined water molecules. At the lowest PAAm concentration of 5%, we found the mean (spherical) pore diameter to lie in the range of 7.3−13.9 nm, taking the completely random Ogston model as a lower bound and the completely ordered lattice model as an upper bound. For the most highly confined water pools, with 40% PAAm, the pore diameter was in the range 1.5−3.8 nm.

The slowdown is not as severe as for water confined on similar length scales in AOT reverse micelles (RMs), which have a charged spherical interface with no connections between different RMs. RM diameters as a function of composition are well known (Table S2).[84,85] Confined water dynamics in RMs have also been extensively studied via PSPP experiments on the O−D stretch of HOD in H_2O.[26−28] Below ∼4 nm in diameter, the RM water pool consists of a single ensemble of water that is uniformly affected by the interface. Orientational dynamics of water in RMs from the previous investigations are summarized in the Supporting Information, Table S3. For the weakest confinement with a relatively low PAAm concentration of 5%, the results differ fundamentally from RMs. In both systems, confinement to a diameter of ∼11 nm resulted in dynamics that are not totally bulk-like. However, the RMs possess a core of bulk water. Water at the interface and close to the interface has very slow orientational relaxation compared to the bulk water core.[27−29] The H-bond network is strongly disrupted by the totally enclosing spherical interface lined with sulfonate anions, affecting the spectral position and vibrational lifetime.[27−29] The geometrical fraction of water molecules at the interface in RMs with the same diameter as a hydrogel pore is much greater (Table S2).

In the hydrogel case on the other hand, confinement affects the pool uniformly. In the hydrogels, water H bonded to the

DOI: 10.1021/jacs.8b03547
J. Am. Chem. Soc. 2018, 140, 9466−9477

polymer fibers is similar to water H bonded to other water molecules as evidenced by the lack of a distinct feature in the spectrum (see Figure 1A). There still exists a 3-dimensional continuous H-bond network throughout the gel. The result is nonbulk water that has uniformly slower orientational relaxation than bulk water.

No bulk water is observed in hydrogels at any of the PAAm concentrations between 5% and 40%, limiting the maximum characteristic or mean pore size. Significantly larger mean pore sizes than those in Table S2 would result in some population of pores with bulk-like water given the large distance to a polymer fiber. Several previous studies based on the diffusion of large macromolecular probes[86,87] and electron microscopy[88,89] have suggested that the pore distribution is about an order of magnitude larger than the ranges proposed here. Such large sizes are not consistent with the orientational dynamics and the other measurements discussed below. While they are likely valid for the distribution of pores accessible to certain macromolecules, it is possible that they are not representative of the entire pore size distribution and may sample only a small fraction of the hydrogel water volume.

3.3. Polarization-Selective Pump−Probe Measurements of $SeCN^-$. The vibrational population decays were extracted from PSPP measurements of $SeCN^-$ in various hydrogels and are shown in Figure 3 (inset). The population decays are reported at the peak center frequencies to avoid complications due to non-Condon effects, which become significant for vibrational modes engaged in H bonds (see Supporting Information, Figure S8).[41,77] Each decay curve was fit well by a single-exponential function. In bulk D_2O, the $SeCN^-$ lifetime is 36.5 ± 0.5 ps.[41,42] Going from 5% to 40% hydrogel, the lifetime shortens from 34.5 ± 0.2 to 29.0 ± 0.1 ps.

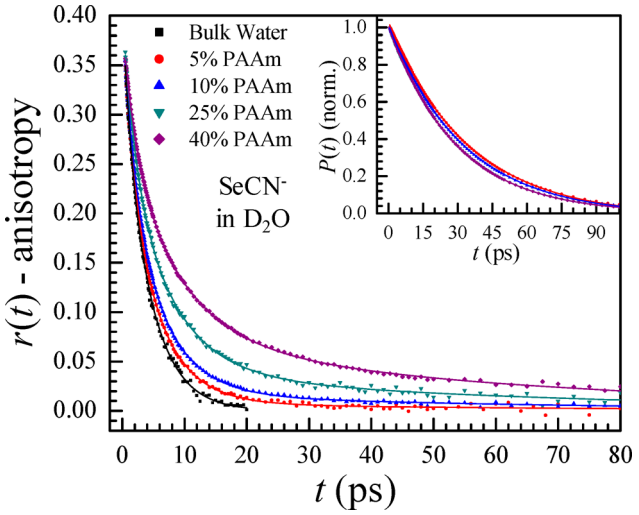

Figure 3. $SeCN^-$ anisotropy decays measured at the peak centers for bulk water and hydrogels (points) with the biexponential fit for bulk water and triexponential fits for hydrogels (solid lines). (Inset) Isotropic pump−probe decays at peak centers (points) for $SeCN^-$ in the 5%, 10%, and 40% PAAm hydrogels with single-exponential fits (solid lines) to determine the vibrational lifetimes.

The relatively small decrease of the vibrational lifetimes suggests that some $SeCN^-$ ions interacting with polymer fibers have a shorter lifetime compared to $SeCN^-$ fully solvated by D_2O. However, none of the population decays can be adequately fitted with a biexponential function. The difference in lifetimes between $SeCN^-$ close to or away from the polymer fibers must be very small if it exists. Though the anisotropy and spectral diffusion dynamics show two dynamical ensembles, the single-exponential vibrational relaxation of $SeCN^-$ in hydrogels indicates that the time-dependent anisotropy decays can be analyzed as the weighted average of each ensemble's dynamics.

Anisotropy decays for $SeCN^-$ are only slightly frequency dependent (Figure S9), suggesting that the spectral distribution of $SeCN^-$ interacting with polymer fibers differs little from probes solvated fully by water. The population ratios are almost the same within the frequency range studied. The anisotropy decay curves of $SeCN^-$ in hydrogels and in bulk water measured at the absorption spectra center frequencies are presented in Figure 3. $SeCN^-$ is a linear anion, with its transition dipole vector along the molecular axis. The anisotropy decay measured from the nitrile stretch directly reports the anion reorientation dynamics. The long vibrational lifetime compared with water allows measurements with good signal-to-noise ratios up to t = 80 ps. In the bulk water solution, the anisotropy decays to zero within 20 ps. As the polymer concentration increases, we observe clear slowing of the major anisotropy decay component as well as an increasing amplitude component with much slower dynamics than $SeCN^-$ in the bulk. The slow component is attributed to the diffusive reorientation of $SeCN^-$ at the PAAm/water interface hindered by the large polymer fibers.

The anisotropy decay of $SeCN^-$ in bulk D_2O has been studied in detail by both experiments and simulations.[41,42] A biexponential decay fits the anisotropy well (Figure 3) and is analyzed with the wobbling-in-a-cone model, similar to the water anisotropy decay in hydrogels discussed above. The orientational dynamics in bulk water also include an inertial cone of θ_i = 11.3 ± 0.1°. Selenocyanate's wobbling and orientational diffusion dynamics in bulk water appear in Table 1. The major contribution to the decay is orientational diffusion on the time scale τ_m = 4.5 ps.

All of the hydrogel anisotropy decays (Figure 3) require triexponential functions to fit. In addition to the two exponential components similarly found in bulk aqueous solutions, there is the much slower exponential decay component assigned to $SeCN^-$ at the PAAm/water interface. We performed a global triexponential fit where the slowest component in hydrogels from T = 5% to 40% share the same time constant. Orientational relaxation of interfacial $SeCN^-$ was assumed to be independent of the polymer concentration, as the interaction of the $SeCN^-$ is very local. The time constants of the other two exponential components and all exponential amplitudes were allowed to vary during fitting procedures. The resulting time constants are shown in Table 1.

The triexponential fit lines shown in Figure 3 agree with the experimental data exceedingly well. The shared slow time constant determined from the global fit is τ_m^{fiber} = 62.5 ± 3.1 ps and is within the error bars of the values determined for each PAAm concentration fit individually. The relative contribution of the slow component amplitude to the overall anisotropy decay is 2.0%, 4.5%, 10.0%, and 18.2%, for T = 5%, 10%, 25%, and 40%, respectively. The values are nearly identical to the geometric fractions of interfacial water in hydrogels shown in Table S2. The amplitude percentage of the slow component tracks the polymer mass concentration proportionally with a slope of 0.44 (R^2 = 0.99), agreeing well with a predicted slope

DOI: 10.1021/jacs.8b03547
J. Am. Chem. Soc. 2018, 140, 9466−9477

of 0.43 (see Supporting Information, Section C). This slow component can therefore be attributed to interfacial $SeCN^-$ with near certainty.

In contrast to $SeCN^-$, water molecules did not display a distinct contribution to reorientation associated with interaction with the polymer fibers. This difference is likely caused by the fundamental difference in the manners in which water and a solute like $SeCN^-$ undergo orientational relaxation. $SeCN^-$ undergoes Gaussian orientational diffusion through continuous small angular fluctuations.[42] When very close to a fiber, these motions will be inhibited by the $SeCN^-$ making close contact with the essentially immovable fiber. In contrast, water undergoes jump reorientation.[55,82] Water orientational relaxation is a concerted process in which many water molecules simultaneously rearrange their hydrogen-bond partners. The result is an ~60° angular jump each time the concerted H-bond reorganization occurs. This is very different from small angular steps that give rise to Gaussian angular diffusion. Water forms H bonds to the fiber, which has both donor and acceptor sites. The water-fiber H-bond strengths are within the range of water−water H-bond strengths as shown by the linear spectrum. A water molecule can break an H bond to the fiber and jump to H bonding to a water molecule in a manner similar to a water−water rearrangement. These water−fiber to water−water jumps are not expected to be identical to jumps involving only water, but if they are similar, the experiment will not reveal the small difference.

The time constants of the other two exponential components of the $SeCN^-$ reorientation are much closer to but still slower than those measured in bulk water. The time constant for complete orientational randomization, τ_m, increases steadily from the bulk value as the PAAm concentration T increases (Table 1). Similar to bulk solutions, these $SeCN^-$ anions also undergo wobbling-in-a-cone dynamics, with both a larger value for the wobbling correlation time τ_c and cone half angle θ_c as compared to the bulk solution. The diffusion times for $SeCN^-$ wobbling in the hydrogels are almost independent of PAAm concentration (Table S1) as τ_c and θ_c do not vary significantly (Table 1). The cone angle in the hydrogels is larger than for $SeCN^-$ in bulk solution. These contributions to orientational relaxation correspond to $SeCN^-$ fully solvated in the water nanopools. The nonbulk time constants show that solvated $SeCN^-$ takes longer to diffusively sample orientations, even for the low concentration of T = 5%.

The degree of slowing down for $SeCN^-$ agrees with that measured from HOD molecules (Table 1). A $SeCN^-$ anion forms a number of hydrogen bonds intimately with the water molecules solvating it.[42] As the water hydrogen-bonding network becomes hindered by the polymer confinement, slowing down the angular jumps necessary for H-bond rearrangement, the $SeCN^-$ anions dissolved in water also slow down. Effectively, the water nanopool viscosity is increasing. Between T = 5% and 40%, the full randomization time constant τ_m increases more than 60% from 5.3 to 8.6 ps. The confinement of the water environment solvating $SeCN^-$ significantly impacts the slower full orientational randomization process. The faster, more local, wobbling dynamics are affected less by increasing confinement.

3.4. 2D IR Measurements of HOD in Water. 2D IR experiments were conducted on bulk water and hydrogels at 5−40% PAAm concentration, interrogating the structural dynamics reported by the O−D stretch mode of the 5% HOD probe. 2D IR measures frequency fluctuations, which are caused by structural changes. Therefore, tracking the correlation function of vibrational frequencies is a measurement of the correlation function of local structures. The H-bond strength and number determines the O−D absorption frequency, so we can equally think of the FFCF as directly characterizing the rate and magnitude of changes in H-bond network structure.

The CLS decays (normalized FFCFs) for all PAAm concentrations and over the full 0.16−2 ps waiting time range are shown in Figure 4A (points). A representative 2D IR spectrum for HOD in the T = 40% hydrogel, taken at waiting time 0.3 ps, is shown in the inset. Biexponential decays, shown as solid lines in Figure 4A, describe each CLS decay extremely well. Similar to the anisotropy decays for HOD in the hydrogels, there is still considerable downward slope at the last few data points collected for each gel sample. Therefore, an additional very slow contribution to the CLS decay is unlikely. The resulting FFCFs are given in Table 2.

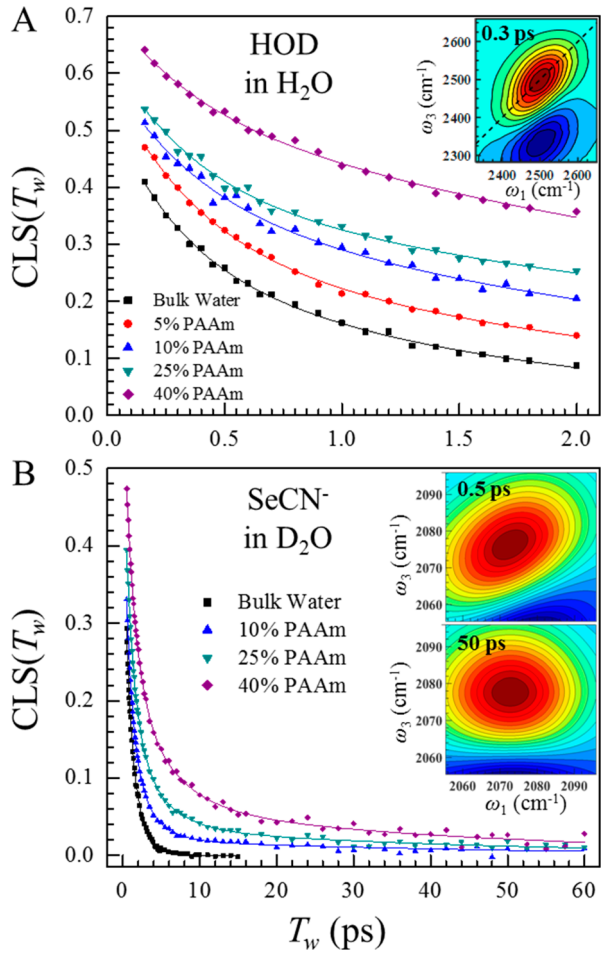

Figure 4. (A) CLS decays for the O−D stretch of HOD in bulk water and hydrogels from 5% to 40% PAAm (points) with biexponential fits to the data (lines). (Inset, A) 2D IR spectrum of HOD in the 40% PAAm gel with a waiting time of 0.3 ps. (B) CLS decays for the nitrile stretch of $SeCN^-$ in bulk water and hydrogels (points) with the biexponential fit for bulk water and triexponential fits for hydrogels (solid lines). (Inset, B) 2D IR spectra of $SeCN^-$ in the 10% PAAm gel at waiting times of 0.5 and 50 ps.

DOI: 10.1021/jacs.8b03547
J. Am. Chem. Soc. 2018, 140, 9466−9477

Table 2. Complete FFCFs, Determined from Fits to the CLS and the Linear Absorption Spectrum, for the O−D Stretch of HOD and the C−N Stretch of $SeCN^-$ in Bulk Solution and Hydrogels

sample	Γ (cm^{-1})[a]	Δ_1 (cm^{-1})	τ_1 (ps)	Δ_2 (cm^{-1})	τ_2 (ps)	τ_{cor} (ps)[b]	Δ_3 (cm^{-1})[c]	τ_3 (ps)
HOD in H_2O								
bulk water	67 ± 7	38 ± 1	0.31 ± 0.05	35 ± 2	1.7 ± 0.2	1.0 ± 0.1		
5% PAAm	62 ± 7	39 ± 2	0.38 ± 0.04	36 ± 2	2.7 ± 0.4	1.4 ± 0.2		
10% PAAm	60 ± 4	34 ± 1	0.38 ± 0.04	41 ± 1	3.3 ± 0.4	2.1 ± 0.2		
25% PAAm	56 ± 4	35 ± 1	0.38 ± 0.04	42 ± 1	4.8 ± 0.8	3.0 ± 0.5		
40% PAAm	46 ± 3	30 ± 2	0.38 ± 0.04	49 ± 1	4.7 ± 0.4	3.5 ± 0.3		
$SeCN^-$ in D_2O								
bulk water	9 ± 1	8.6 ± 0.4	0.5 ± 0.1	10.7 ± 0.5	1.4 ± 0.1	1.0 ± 0.1		
10% PAAm	11 ± 1	10.1 ± 0.6	0.9 ± 0.1	6 ± 1	2.6 ± 0.5	1.3 ± 0.2	2.5 ± 0.1	44 ± 4
25% PAAm	11 ± 1	9.9 ± 0.3	1.1 ± 0.1	6.5 ± 0.7	3.9 ± 0.6	1.9 ± 0.3	3.2 ± 0.1	44 ± 4
40% PAAm	10 ± 1	9.5 ± 0.3	1.3 ± 0.1	7.0 ± 0.4	5.0 ± 0.6	2.6 ± 0.3	4.1 ± 0.2	44 ± 4

[a]$\Gamma = 1/(\pi T_2)$ is the fwhm of the Lorentzian homogeneous line shape, with T_2 being the total dephasing time. The frequency fluctuation amplitudes Δ_k are standard deviations of the Gaussian inhomogeneous line shapes, which are convolved for the total inhomogeneous contribution: $\Delta^2_{total} = \sum_k \Delta^2_k$. The fwhm of the inhomogeneous line shape is given by $\Delta_{fwhm} = 2.355 \times \Delta_{total}$. [b]Integrated correlation time calculated for the T_w-dependent part of FFCF decay for the fully solvated HOD or $SeCN^-$ probes but excluding fiber-associated $SeCN^-$ ions. [c]Contribution to inhomogeneous band from polymer fiber-associated probe molecules.

Additional examples of 2D IR spectra for HOD in the hydrogels, illustrating the center lines for CLS determination, are provided in the Supporting Information, Figure S6. The center lines had no deviations from linearity over the center regions of the 2D spectra. A band consisting of two ensembles with distinct dynamics would show significant curvature in the center line.[90] This provides additional evidence that the entire water nanopool behaves as a single dynamical ensemble.

For bulk water, the O−D stretch spectral diffusion occurs on two well-established time scales of 0.4 ± 0.1 and 1.7 ± 0.1 ps,[15,16,40] which the present measurement reproduces within the error (Table 2). The nature of the two decay components has been identified from molecular dynamics (MD) simulations. The fast component is caused by very local hydrogen-bond length fluctuations with also a small contribution from angular fluctuations.[15,16,56,75] The slower component is caused by the complete randomization of the H-bond network.[15,16,56,75] All of the hydrogel samples display a fast component that is within the error bars the same as that found for bulk water (Table 2). The hydrogel does not influence the very local H-bond motions. When fit independently, the fast components for the hydrogel samples (T = 5−40%) did not differ from each other. To better determine the long time constants in the presence of experimental error and with a limited waiting time range, the value for τ_1 was shared between the data sets, with the remaining biexponential parameters freely varied.

In analogy to bulk water, the longer time scale component should result from complete randomization of the H-bond network's structure, including the breaking and reformation of H bonds with new donors and acceptors.[15,16,56,75] The slow component increases steadily from 1.7 ps for bulk water to ∼5 ps at the highest PAAm concentrations (Table 2). To observe the clear trend of H-bond network rearrangement slowing down with increasing T, Table 2 also includes the integrated FFCF correlation time, τ_{cor}, which progressively increases from 1.0 ps for bulk water to 3.5 ps for 40% PAAm. The slowing of H-bond rearrangement with increasing polymer concentration demonstrates the influence of nanoconfinement in the gel on the water dynamics.

While the HOD absorption band has essentially the same width for all hydrogels, the contributions to this width vary with PAAm concentration. The homogeneous line width Γ decreases systematically as T increases (Table 2), which is also evident in Figure 4 from the increasing initial CLS value. Ultrafast fluctuations with $\Delta \times \tau \ll 1$ result in a motionally narrowed component, contributing $\Gamma^* = \Delta^2\tau/\pi$ to the homogeneous width. As the polymer concentration in the gels increases, these fluctuations must become faster in τ or sample less of a spectral range in Δ to cause the decreasing trend in Γ. It is more likely that a decrease in Δ is responsible for the decrease in Γ as T increases, rather than an acceleration in τ while all other dynamics slow down.

H-bond dynamics on the fastest measured time scale of ∼0.4 ps have a trend toward a smaller amplitude of Δ_1 as the PAAm concentration is increased. The decreases in Γ and Δ_1 are made up for by a clear increase in Δ_2 as T increases. In addition to the H-bond rearrangement time scale becoming slower (from 1.7 ps for the bulk to ∼5 ps at 40% PAAm), more of the structural relaxation depends on these slower H-bond network fluctuations.

As discussed in section 3.2, the hydrogels have water pools of characteristic sizes between ∼11 nm for the lowest PAAm concentrations and ∼2.6 nm for the highest PAAm concentrations based on two simple models (see also Supporting Information, Table S2). The slowing of the H-bond network rearrangement at all PAAm concentrations gives further indications that these size calculations are of the correct scale, as the water properties must approach those of the bulk for large characteristic water pool sizes.

3.5. 2D IR Measurements of $SeCN^-$. 2D IR measurements were performed on the nitrile stretch mode of $SeCN^-$ for hydrogels with T = 10%, 25%, and 40%. The measured CLS decay curves of $SeCN^-$ dissolved in bulk water and in the PAAm hydrogels with various concentrations T are compared in Figure 4B (points). In bulk water, the biexponential spectral diffusion of $SeCN^-$ tracks the randomization of the water hydrogen-bonding network.[41,42] In aqueous solution, a $SeCN^-$ anion forms hydrogen bonds with water molecules. The instantaneous vibrational frequency of a $SeCN^-$ anion is sensitive to the hydrogen-bonding configuration.[42] The faster time constant associated with bulk water−$SeCN^-$ hydrogen-bond fluctuations is τ_1 = 0.5 ± 0.1 ps, and the slower time constant associated with complete hydrogen-bonding config-

DOI: 10.1021/jacs.8b03547
J. Am. Chem. Soc. 2018, 140, 9466−9477

uration randomization is τ_2 = 1.4 ± 0.1 ps, in good agreement with previous measurements and molecular dynamics simulations.[29,41,42] The fitting parameters are listed in Table 2. These time constants are very close to the spectral diffusion time constants of HOD measured in H_2O discussed above, essentially within the error bars. As the water hydrogen-bond configurations randomize, $SeCN^-$ samples all configurations that give rise to the inhomogeneously broadened absorption line.

It was possible to measure the spectral diffusion dynamics to ~60 ps because of the long vibrational lifetime of the nitrile stretching mode. Example 2D IR spectra for the T = 10% sample at short and very long waiting times are shown in the inset to Figure 4B. Additional 2D IR spectra for different polymer concentrations and various waiting times are available in the Supporting Information, Figure S7.

In the hydrogels, the CLS decay curves were fit to triexponentials (Figure 4B, solid lines). Visual inspection of the data in Figure 4B shows a slow, small amplitude, spectral diffusion term lasting tens of picoseconds in hydrogels. Similar to the treatment of anisotropy decays, we performed a global fit with the third exponential term sharing the same time constant across hydrogels with different T. This shared time constant is τ_3 = 44 ± 4 ps, and we assign it to the interfacial $SeCN^-$ interacting with polymer fibers (see Table 2). Spectral diffusion of the OD stretch of HOD has a slowest component of ~5 ps in the highest concentration PAAm gels. Therefore, the spectral diffusion dynamics of interfacial $SeCN^-$ do not fully sample their inhomogeneous line widths on the time scale during which essentially all water molecules in hydrogels have randomized their hydrogen-bond configurations. As shown by the peak shift of linear absorption spectra in Figure 1B, interactions between $SeCN^-$ and PAAm polymer fibers cause inhomogeneous broadening in addition to the interactions between $SeCN^-$ and water. Sampling of this additional inhomogeneity involves significantly slower motions. $SeCN^-$ ions associated with the fiber may have to move relative to the fiber or leave the fiber to sample this component of the inhomogeneous line. The contribution to the total inhomogeneous line from the interfacial component, Δ_3, increases as T goes from 5% to 40% because a larger fraction of $SeCN^-$ ions are adjacent to polymer fiber, as was discussed for the anisotropy decays above.

The shortest and middle time constants τ_1 and τ_2 (Table 2) are associated with the dynamics of $SeCN^-$ fully solvated by water in the hydrogel pores. In the gels, τ_1 and τ_2 are both significantly slower than values for $SeCN^-$ in bulk water. As T increases from 5% to 40%, τ_1 increases from 0.9 ± 0.1 to 1.3 ± 0.1 ps and τ_2 increases from 2.6 ± 0.5 to 5.0 ± 0.6 ps. The slower spectral diffusion term τ_2 is more sensitive to the polymer concentration than the faster term τ_1. The τ_2 values are within experimental error of the values found for HOD in H_2O for the same polymer concentration. Therefore, in the hydrogel pores, the complete spectral diffusion time scale of $SeCN^-$ vibrational frequencies still tracks the polymer-confined H-bond rearrangement dynamics of the surrounding water molecules. These structural dynamics result in the sampling of different water−anion hydrogen-bond configurations, modulating the frequency of the $SeCN^-$ stretch. As the water hydrogen-bonding network in this confined, nonbulk, state takes more time to fully sample all configurations, the spectral diffusion dynamics of the dissolved anion are slowed down accordingly. Comparing to the anions at the polymer/water interface, the structural fluctuations experienced by $SeCN^-$ fully solvated by water are nearly an order of magnitude faster than those associated with the fibers.

The faster time scale fluctuations, τ_1, change with polymer concentration for the $SeCN^-$ probe, while they are constant within error for HOD. For HOD, these fast dynamics are caused by very local H-bond length fluctuations associated with the D, which are independent of the change in the global H-bond randomization dynamics. However, the nitrile can make several H bonds with water.[42] Apparently the multiple H bonds and possibly the much larger mass of $SeCN^-$ compared to HOD result in greater sensitivity to the polymer induced changes in the H-bond network.

4. CONCLUDING REMARKS

In this paper we applied ultrafast PSPP IR spectroscopy and 2D IR spectroscopy to investigate the dynamics of water confined in the pores of PAAm hydrogels using two different probe molecules: water (HOD) and the selenocyanate ion ($SeCN^-$). For hydrogels studied (polymer concentration 5% and above) the reorientation dynamics of the probes reported by the anisotropy decay and the hydrogen-bonding network reorganization dynamics reported by the spectral diffusion have slowed down significantly from bulk water. Both HOD and the solvated $SeCN^-$ were found to report very similar slowing of the H-bond dynamics. The water dynamics become increasingly slow as the polymer mass concentration increases.

From the spectroscopic data measured from HOD molecules, the entire hydrogen-bonding network of water molecules in hydrogels slows down as a single ensemble without a distinction between a "shell" of water at the polymer fibers and "core" water further away from the fibers. This is attributed to water's unique ability to form three-dimensional hydrogen-bonding networks and the structure of PAAm, which is neutral in charge and has H-bond donors and acceptors along its fibers that do not disrupt the water network. In contrast, the $SeCN^-$ spectroscopic observables exhibit two-component dynamics, where we assign the faster components to anions fully solvated in water pools and another much slower component on the time scale of tens of picoseconds to anions strongly interacting with the polymer fibers.

Using both the solvent (HOD) and a dissolved solute ($SeCN^-$) as a probe, no bulk-like water was detected in hydrogels between the lowest (5%) and the highest (40%) PAAm concentrations studied here; all water molecules are affected by gelation to some extent. Estimates of the pore sizes were calculated using simple limiting models for the polymer network topography.[83] Comparison to the well-known sizes of AOT reverse micelles[84,85] and their confinement effects on water dynamics[26−28] showed these hydrogel pore size estimates from the Ogston model and the cubic lattice model were reasonable for the dynamical slowing observed in the data. Even at PAAm concentrations as low as 5%, the maximum pore diameter was found to be less than 14 nm using the cubic lattice model, in contrast to some other experimental methods that have suggested much larger average pore sizes.[86−89] Our results are in agreement with recent work, in which the average pore diameter of PAAm with T = 4% and C = 3.3% was measured as 11 nm by modeling the diffusion of polymeric dextran molecules in PAAm.[91]

The global water dynamics in the hydrogel nanopools observed here differ from water in some other polymer-crowded environments. Recent studies by Cho and Kubarych

DOI: 10.1021/jacs.8b03547
J. Am. Chem. Soc. 2018, 140, 9466−9477

examined the dynamics of water (HOD) and H-bond-sensitive vibrational probe molecules (azide and a metal carbonyl complex) in solutions of polyethylene glycol (PEG) as a model for crowded cytoplasm-like environments.[43,50] Both groups found a large population of bulk-like water even in highly crowded samples. These studies suggested PEG chains may be special in their ability to take on conformations that minimally disrupt the 3D H-bond network of water. PAAm as the basis of the hydrogels studied in the present work, even though it provides H-bond donor and acceptor sites, forms a far more perturbative polymer network when cross-linked as seen in the slowing of the global water dynamics. This is consistent with the fact that even low-concentration solutions of PAAm in water form hydrogels rather than liquid solutions. In hydrogels, the specific dynamics of confined water may depend much on the chemical structure of polymer side chains. However, it is important to note that studies of water confined in reverse micelles showed only small differences between reverse micelles with charged and neutral interfaces.[92] To further understand the dynamics in hydrogel pores, the results here could be compared with other hydrogels containing different side chain groups, such as poly(vinyl alcohol), polyvinyl methyl ether, and poly-*N*-isopropylacrylamide. There are likely to be significant differences in water dynamics between polymers that are both H-bond donors and acceptors, as studied here, and polymers that are not.

The results presented above provide direct time-resolved measurements of the dynamics of water and a small solute in hydrogels on the fast time scales of molecular motions. This quantitative explication of the confined water H-bond network dynamics can provide benchmarks for simulations on polymer-crowded water. Biomolecule behavior can depend strongly on the solvating water dynamics,[51] which is much different in hydrogels than in the bulk. The results enhance our understanding of hydrogels and may facilitate future applications of this class of materials as novel transport media and reaction media.

■ ASSOCIATED CONTENT

Supporting Information

The Supporting Information is available free of charge on the ACS Publications website at DOI: 10.1021/jacs.8b03547.

Experimental methods for linear and time-resolved IR spectroscopy, details on the wobbling-in-a-cone model, estimation of pore sizes and geometric fraction of interfacial molecules in hydrogels, FFCF analysis methods, analysis of frequency-dependent PSPP measurements of HOD and $SeCN^-$ probes, and additional 2D IR spectra (PDF)

■ AUTHOR INFORMATION

Corresponding Author

*fayer@stanford.edu

ORCID

Chang Yan: 0000-0001-9735-3002

Michael D. Fayer: 0000-0002-0021-1815

Present Address

‡Department of Chemistry, University of California, Berkeley, California 94720, United States.

Author Contributions

†C.Y. and P.L.K. contributed equally to this work.

Notes

The authors declare no competing financial interest.

■ ACKNOWLEDGMENTS

This work was supported by the Air Force Office of Scientific Research grant no. FA9550-16-1-0104 (C.Y. and M.D.F.) and by the Division of Chemical Sciences, Geosciences, and Biosciences, Office of Basic Energy Sciences of the U.S. Department of Energy (DOE) grant no. DEFG03-84ER13251 (P.L.K., R.Y., and M.D.F.). P.L.K. also acknowledges partial financial support through an ARCS fellowship. We thank Steven Yamada for assistance with the determination of FFCF parameters for the $SeCN^-$ probe.

■ REFERENCES

(1) Ahmed, E. M. *J. Adv. Res.* **2015**, *6*, 105−121.
(2) Hoffman, A. S. *Adv. Drug Delivery Rev.* **2012**, *64*, 18−23.
(3) Drury, J. L.; Mooney, D. J. *Biomaterials* **2003**, *24*, 4337−4351.
(4) Lee, K. Y.; Mooney, D. J. *Chem. Rev.* **2001**, *101*, 1869−1879.
(5) Kamoun, E. A.; Kenawy, E. R. S.; Chen, X. *J. Adv. Res.* **2017**, *8*, 217−233.
(6) Nicolson, P. C.; Vogt, J. *Biomaterials* **2001**, *22*, 3273−3283.
(7) Chrambach, A.; Rodbard, D. *Science* **1971**, *172*, 440−451.
(8) Flavel, B. S.; Moore, K. E.; Pfohl, M.; Kappes, M. M.; Hennrich, F. *ACS Nano* **2014**, *8*, 9687−9687.
(9) Fawcett, J. S.; Morris, C. J. O. R. *Sep. Sci.* **1966**, *1*, 9−26.
(10) Alarcon, C. D. H.; Pennadam, S.; Alexander, C. *Chem. Soc. Rev.* **2005**, *34*, 276−285.
(11) Stuart, M. A. C.; Huck, W. T. S.; Genzer, J.; Muller, M.; Ober, C.; Stamm, M.; Sukhorukov, G. B.; Szleifer, I.; Tsukruk, V. V.; Urban, M.; Winnik, F.; Zauscher, S.; Luzinov, I.; Minko, S. *Nat. Mater.* **2010**, *9*, 101−113.
(12) Phadke, A.; Zhang, C.; Arman, B.; Hsu, C. C.; Mashelkar, R. A.; Lele, A. K.; Tauber, M. J.; Arya, G.; Varghese, S. *Proc. Natl. Acad. Sci. U. S. A.* **2012**, *109*, 4383−4388.
(13) Taylor, D. L.; Panhuis, M. I. H. *Adv. Mater.* **2016**, *28*, 9060−9093.
(14) Nakamura, H.; Lee, A. A.; Afshar, A. S.; Watanabe, S.; Rho, E.; Razavi, S.; Suarez, A.; Lin, Y.-C.; Tanigawa, M.; Huang, B. *Nat. Mater.* **2018**, *17*, 79.
(15) Asbury, J. B.; Steinel, T.; Kwak, K.; Corcelli, S. A.; Lawrence, C. P.; Skinner, J. L.; Fayer, M. D. *J. Chem. Phys.* **2004**, *121*, 12431.
(16) Asbury, J. B.; Steinel, T.; Stromberg, C.; Corcelli, S. A.; Lawrence, C. P.; Skinner, J. L.; Fayer, M. D. *J. Phys. Chem. A* **2004**, *108*, 1107−1119.
(17) Fecko, C. J.; Loparo, J. J.; Roberts, S. T.; Tokmakoff, A. *J. Chem. Phys.* **2005**, *122*, 054506−054518.
(18) Park, S.; Fayer, M. D. *Proc. Natl. Acad. Sci. U. S. A.* **2007**, *104*, 16731−16738.
(19) Laage, D.; Stirnemann, G.; Sterpone, F.; Rey, R.; Hynes, J. T. *Annu. Rev. Phys. Chem.* **2011**, *62*, 395−416.
(20) Roberts, S. T.; Ramasesha, K.; Tokmakoff, A. *Acc. Chem. Res.* **2009**, *42*, 1239−1249.
(21) Nihonyanagi, S.; Yamaguchi, S.; Tahara, T. *Chem. Rev.* **2017**, *117*, 10665−10693.
(22) Yan, C.; Thomaz, J. E.; Wang, Y. L.; Nishida, J.; Yuan, R. F.; Breen, J. P.; Fayer, M. D. *J. Am. Chem. Soc.* **2017**, *139*, 16518−16527.
(23) King, J. T.; Kubarych, K. J. *J. Am. Chem. Soc.* **2012**, *134*, 18705−18712.
(24) Sterpone, F.; Stirnemann, G.; Laage, D. *J. Am. Chem. Soc.* **2012**, *134*, 4116−4119.
(25) Laage, D.; Elsaesser, T.; Hynes, J. T. *Chem. Rev.* **2017**, *117*, 10694−10725.
(26) Moilanen, D. E.; Fenn, E. E.; Wong, D.; Fayer, M. D. *J. Am. Chem. Soc.* **2009**, *131*, 8318−8328.
(27) Moilanen, D. E.; Fenn, E. E.; Wong, D.; Fayer, M. D. *J. Phys. Chem. B* **2009**, *113*, 8560−8568.

DOI: 10.1021/jacs.8b03547
J. Am. Chem. Soc. 2018, 140, 9466−9477

(28) Moilanen, D. E.; Fenn, E. E.; Wong, D.; Fayer, M. D. *J. Chem. Phys.* **2009**, *131*, 014704.
(29) Yuan, R. F.; Yan, C.; Nishida, J.; Fayer, M. D. *J. Phys. Chem. B* **2017**, *121*, 4530−4537.
(30) Levinger, N. E.; Swafford, L. A. *Annu. Rev. Phys. Chem.* **2009**, *60*, 385−406.
(31) Nandi, N.; Bhattacharyya, K.; Bagchi, B. *Chem. Rev.* **2000**, *100*, 2013−2045.
(32) Alam, T. M.; Childress, K. K.; Pastoor, K.; Rice, C. V. *J. Polym. Sci., Part B: Polym. Phys.* **2014**, *52*, 1521−1527.
(33) Deriu, A.; Cavatorta, F.; Cabrini, D.; Carlile, C. J.; Middendorf, H. D. *Europhys. Lett.* **1993**, *24*, 351−357.
(34) Bhattacharyya, K.; Bagchi, B. *J. Phys. Chem. A* **2000**, *104*, 10603−10613.
(35) Netz, P. A.; Dorfmuller, T. *J. Phys. Chem. B* **1998**, *102*, 4875−4886.
(36) Tamai, Y.; Tanaka, H.; Nakanishi, K. *Mol. Simul.* **1996**, *16*, 359−374.
(37) Datta, A.; Das, S.; Mandal, D.; Pal, S. K.; Bhattacharyya, K. *Langmuir* **1997**, *13*, 6922−6926.
(38) Ghosh, S.; Adhikari, A.; Mandal, U.; Dey, S.; Bhattacharyya, K. *J. Phys. Chem. C* **2007**, *111*, 8775−8780.
(39) Rezus, Y. L. A.; Bakker, H. J. *J. Chem. Phys.* **2005**, *123*, 114502.
(40) Park, S.; Moilanen, D. E.; Fayer, M. D. *J. Phys. Chem. B* **2008**, *112*, 5279−5290.
(41) Yuan, R. F.; Yan, C.; Tamimi, A.; Fayer, M. D. *J. Phys. Chem. B* **2015**, *119*, 13407−13415.
(42) Yamada, S. A.; Thompson, W. H.; Fayer, M. D. *J. Chem. Phys.* **2017**, *146*, 234501.
(43) Verma, P. K.; Kundu, A.; Ha, J. H.; Cho, M. *J. Am. Chem. Soc.* **2016**, *138*, 16081−16088.
(44) Fenn, E. E.; Wong, D. B.; Fayer, M. D. *J. Chem. Phys.* **2011**, *134*, 054512.
(45) Osborne, D. G.; Dunbar, J. A.; Lapping, J. G.; White, A. M.; Kubarych, K. J. *J. Phys. Chem. B* **2013**, *117*, 15407−15414.
(46) Zhao, W.; Moilanen, D. E.; Fenn, E. E.; Fayer, M. D. *J. Am. Chem. Soc.* **2008**, *130*, 13927−13937.
(47) Giammanco, C. H.; Wong, D. B.; Fayer, M. D. *J. Phys. Chem. B* **2012**, *116*, 13781−13792.
(48) Bakker, H. J. *Chem. Rev.* **2008**, *108*, 1456−1473.
(49) Kramer, P. L.; Giammanco, C. H.; Fayer, M. D. *J. Chem. Phys.* **2015**, *142*, 212408.
(50) Daley, K. R.; Kubarych, K. J. *J. Phys. Chem. B* **2017**, *121*, 10574−10582.
(51) Ball, P. *Chem. Rev.* **2008**, *108*, 74−108.
(52) Tan, H.-S.; Piletic, I. R.; Riter, R. E.; Levinger, N. E.; Fayer, M. D. *Phys. Rev. Lett.* **2005**, *94*, 057405.
(53) Park, S.; Kwak, K.; Fayer, M. D. *Laser Phys. Lett.* **2007**, *4*, 704−718.
(54) Hamm, P.; Zanni, M. T. *Concepts and Methods of 2D Infrared Spectroscopy*; Cambridge University Press: Cambridge, New York, 2011.
(55) Laage, D.; Hynes, J. T. *Science* **2006**, *311*, 832−835.
(56) Corcelli, S.; Lawrence, C. P.; Skinner, J. L. *J. Chem. Phys.* **2004**, *120*, 8107−8117.
(57) Mukamel, S. *Principles of Nonlinear Optical Spectroscopy*; Oxford University Press: New York, 1995.
(58) Tan, H.-S.; Piletic, I. R.; Fayer, M. D. *J. Opt. Soc. Am. B* **2005**, *22*, 2009−2017.
(59) Tokmakoff, A. *J. Chem. Phys.* **1996**, *105*, 1−12.
(60) Kinosita, K.; Kawato, S.; Ikegami, A. *Biophys. J.* **1977**, *20*, 289−305.
(61) Kinosita, K.; Ikegami, A.; Kawato, S. *Biophys. J.* **1982**, *37*, 461−464.
(62) Lipari, G.; Szabo, A. *Biophys. J.* **1980**, *30*, 489−506.
(63) Wang, C. C.; Pecora, R. *J. Chem. Phys.* **1980**, *72*, 5333−5340.
(64) Otting, G.; Liepinsh, E.; Wuthrich, K. *Science* **1991**, *254*, 974−980.
(65) Zhang, Z.; Berkowitz, M. L. *J. Phys. Chem. B* **2009**, *113*, 7676−7680.
(66) Spry, D. B.; Goun, A.; Glusac, K.; Moilanen, D. E.; Fayer, M. D. *J. Am. Chem. Soc.* **2007**, *129*, 8122−8130.
(67) Douhal, A.; Angulo, G.; Gil, M.; Organero, J. A.; Sanz, M.; Tormo, L. *J. Phys. Chem. B* **2007**, *111*, 5487−5493.
(68) Petersen, M. K.; Hatt, A. J.; Voth, G. A. *J. Phys. Chem. B* **2008**, *112*, 7754−7761.
(69) Kramer, P. L.; Nishida, J.; Fayer, M. D. *J. Chem. Phys.* **2015**, *143*, 124505.
(70) van der Post, S. T.; Tielrooij, K.-J.; Hunger, J.; Backus, E. H.; Bakker, H. J. *Faraday Discuss.* **2013**, *160*, 171−189.
(71) Kwak, K.; Park, S.; Finkelstein, I. J.; Fayer, M. D. *J. Chem. Phys.* **2007**, *127*, 124503.
(72) Kwak, K.; Rosenfeld, D. E.; Fayer, M. D. *J. Chem. Phys.* **2008**, *128*, 204505.
(73) Guo, Q.; Pagano, P.; Li, Y.-L.; Kohen, A.; Cheatum, C. M. *J. Chem. Phys.* **2015**, *142*, 212427.
(74) Corcelli, S.; Skinner, J. L. *J. Phys. Chem. A* **2005**, *109*, 6154−6165.
(75) Lawrence, C. P.; Skinner, J. L. *J. Chem. Phys.* **2003**, *118*, 264−272.
(76) Koshimo, A. *J. Appl. Polym. Sci.* **1965**, *9*, 81−90.
(77) Schmidt, J. R.; Corcelli, S. A.; Skinner, J. L. *J. Chem. Phys.* **2005**, *123*, 044513.
(78) Kenkre, V. M.; Tokmakoff, A.; Fayer, M. D. *J. Chem. Phys.* **1994**, *101*, 10618−10629.
(79) Wong, D. B.; Giammanco, C. H.; Fenn, E. E.; Fayer, M. D. *J. Phys. Chem. B* **2013**, *117*, 623−635.
(80) Moilanen, D. E.; Fenn, E. E.; Lin, Y. S.; Skinner, J. L.; Bagchi, B.; Fayer, M. D. *Proc. Natl. Acad. Sci. U. S. A.* **2008**, *105*, 5295−5300.
(81) Tan, H.-S.; Piletic, I. R.; Fayer, M. D. *J. Chem. Phys.* **2005**, *122*, 174501.
(82) Laage, D.; Hynes, J. T. *J. Phys. Chem. B* **2008**, *112*, 14230−14242.
(83) Ogston, A. G. *Trans. Faraday Soc.* **1958**, *54*, 1754−1757.
(84) Kinugasa, T.; Kondo, A.; Nishimura, S.; Miyauchi, Y.; Nishii, Y.; Watanabe, K.; Takeuchi, H. *Colloids Surf., A* **2002**, *204*, 193−199.
(85) Zulauf, M.; Eicke, H. F. *J. Phys. Chem.* **1979**, *83*, 480−486.
(86) Holmes, D. L.; Stellwagen, N. C. *Electrophoresis* **1991**, *12*, 253−263.
(87) Holmes, D. L.; Stellwagen, N. C. *Electrophoresis* **1991**, *12*, 612−619.
(88) Rüchel, R.; Brager, M. D. *Anal. Biochem.* **1975**, *68*, 415−428.
(89) Rüchel, R.; Steere, R. L.; Erbe, E. F. *J. Chromatogr. A* **1978**, *166*, 563−575.
(90) Fenn, E. E.; Fayer, M. D. *J. Chem. Phys.* **2011**, *135*, 074502.
(91) Sandrin, D.; Wagner, D.; Sitta, C.; Thoma, R.; Felekyan, S.; Hermes, H.; Janiak, C.; de Sousa Amadeu, N.; Kühnemuth, R.; Löwen, H. *Phys. Chem. Chem. Phys.* **2016**, *18*, 12860−12876.
(92) Fenn, E. E.; Wong, D. B.; Fayer, M. D. *Proc. Natl. Acad. Sci. U. S. A.* **2009**, *106*, 15243−15248.

DOI: 10.1021/jacs.8b03547
J. Am. Chem. Soc. 2018, 140, 9466−9477